An Indirect Effect of Ice Nuclei on Atmospheric Radiation

XIPING ZENG,*,+ WEI-KUO TAO,+ MINGHUA ZHANG,# ARTHUR Y. HOU,+ SHAOCHENG XIE,@ STEPHEN LANG,+,& XIAOWEN LI,*,+ DAVID O'C. STARR,+ XIAOFAN LI,** AND JOANNE SIMPSON+

*Goddard Earth Sciences and Technology Center, University of Maryland, Baltimore County, Baltimore, Maryland
+Laboratory for Atmospheres, NASA Goddard Space Flight Center, Greenbelt, Maryland
#School of Marine and Atmospheric Sciences, Stony Brook University, New York
@Atmospheric Sciences Division, Lawrence Livermore National Laboratory, Livermore, California
&Science Systems and Applications Inc., Lanham, Maryland
**National Environmental Satellite, Data, and Information Service, NOAA, Camp Spring, Maryland

(Manuscript received 29 February 2008, in final form 16 June 2008)

ABSTRACT

A three-dimensional cloud-resolving model (CRM) with observed large-scale forcing is used to study how ice nuclei (IN) affect the net radiative flux at the top of the atmosphere (TOA). In all the numerical experiments carried out, the cloud ice content in the upper troposphere increases with IN number concentration via the Bergeron process. As a result, the upward solar flux at the TOA increases whereas the infrared one decreases. Because of the opposite response of the two fluxes to IN concentration, the sensitivity of the net radiative flux at the TOA to IN concentration varies from one case to another.

Six tropical and three midlatitudinal field campaigns provide data to model the effect of IN on radiation in different latitudes. Classifying the CRM simulations into tropical and midlatitudinal and then comparing the two types reveals that the indirect effect of IN on radiation is greater in the middle latitudes than in the tropics. Furthermore, comparisons between model results and observations suggest that observational IN data are necessary to evaluate long-term CRM simulations.

1. Introduction

Clouds greatly impact the global energy cycle via radiation (Hartmann et al. 1992) and thus play an important role in climate change. However, understanding this role is still a challenge (Charney 1979) because the cloud time scale is much shorter than that of climate variation. Because atmospheric aerosols affect a cloud on a time scale much shorter than that of a cloud, the National Research Council (NRC; National Research Council 2005) listed the indirect effect of aerosols on climate change as the largest of all the uncertainties about global climate (or radiative) forcing. Here, the "indirect effect" accounts for the contribution of aerosols to radiation through clouds and their associated processes, such as precipitation efficiency (PE).

Baker (1997) and Lohmann and Feichter (2005) analyzed the possible effects of cloud microphysics on climate variation and identified two major gaps between cloud microphysics and climate variation: The first is the linkage between the aerosol particle and cloud (ice) particle populations, and the second is the connection between precipitation formation in the middle troposphere and the radiative roles of mixed-phase clouds. In this study, long-term cloud-resolving model (CRM) simulations are utilized to bridge the two gaps and further study the indirect effect of ice nuclei (IN; a form of aerosols) on radiative forcing or the net radiative flux at the top of the atmosphere (TOA).

a. CRM simulations

CRMs, when representing cloud microphysics and other subgrid processes properly, can simulate clouds well (e.g., Tao 2003). They have been used to explore the effects of cloud microphysics on cloud ensembles (or climatic states) through one of three different modeling frameworks. In the first, CRMs are run until they reach a quasi-equilibrium state to study radiative–convective equilibrium (e.g., Robe and Emanuel 1996,

Corresponding author address: Dr. Xiping Zeng, C423, Bldg. 33, Mail Code 613.1, NASA Goddard Space Flight Center, Greenbelt, MD 20771.
E-mail: zeng@agnes.gsfc.nasa.gov

DOI: 10.1175/2008JAS2778.1

© 2009 American Meteorological Society

2001; Tompkins and Craig 1998; Zeng and Raymond 1999; Bretherton et al. 2005; Cohen and Craig 2006). Although the framework involves no large-scale circulations, this kind of modeling study has provided a means for understanding the effect of clouds on equilibrium states, such as the sensitivity of equilibrium states to vertical wind shear and cloud microphysics (Robe and Emanuel 2001; Bretherton et al. 2005; Cohen and Craig 2006).

In the second framework, CRM simulations are used to address the coupling between clouds and large-scale circulations in the context of either the weak temperature gradient approximation of Sobel and Bretherton (2000) and Bretherton and Sobel (2003) (Raymond and Zeng 2005) or of a general circulation model (Grabowski 2001; Khairoutdinov and Randall 2001; Randall et al. 2003; Khairoutdinov et al. 2005; Tao et al. 2009). This type of study has shown the sensitivity of cloud ensembles to environmental variables such as the horizontal gradient of sea surface temperature.

In the third framework, CRMs are employed to study the response of clouds to observed large-scale forcing (e.g., Lau et al. 1994; Sui et al. 1994; Xu and Randall 1996; Tao et al. 1999; Blossey et al. 2007; Lang et al. 2007; Zeng et al. 2007a, 2008). This type of modeling study has shown the sensitivity of cloud ensembles to cloud microphysics parameterization (e.g., Xu and Randall 1996; Grabowski et al. 1998; Wu et al. 1999; Hong et al. 2004; Lang et al. 2007; Zeng et al. 2007a). Unlike the first two frameworks, this last one provides an opportunity to evaluate CRMs as well as their cloud microphysics parameterization.

Current modeling studies using the three frameworks have shown the sensitivity of cloud ensembles to cloud microphysics (e.g., Xu and Randall 1996; Grabowski et al. 1998; Wu et al. 1999; Bretherton et al. 2005; Ekman et al. 2007; Phillips et al. 2007; Zhang et al. 2007; Zeng et al. 2008). Because clouds modulate radiation, it is expected that radiation would be sensitive to cloud microphysics (Wu et al. 2008). However, previous CRM studies that explored the effect of cloud microphysics on radiation focused on cloud–radiation interaction (e.g., Sui et al. 1994; Lau et al. 1994; Tao et al. 1996; Grabowski et al. 1999; Wu et al. 1999; Wu and Moncrieff 2001). So far, few CRM simulations have addressed the effect of IN on radiative forcing.

b. *Effect of IN on cloud ensembles*

IN concentrations vary greatly with air temperature (e.g., Fletcher 1962; Meyers et al. 1992). Because they compose about one part of 10^8 aerosol particles at a temperature of $-15°C$ (Baker 1997), their direct effect on radiation is negligible. Nevertheless, they can significantly impact cloud ensembles (e.g., Ekman et al. 2007; Phillips et al. 2007, Zeng et al. 2007b, 2008), which can in turn impact atmospheric radiation. Hence, the effect of IN on radiation via clouds is expected to be large.

The present paper, with the aid of CRM simulations, addresses the indirect effect of IN on radiation. It consists of six sections. Section 2 describes the CRM and the parameterization of the Bergeron process. Section 3 introduces the large-scale forcing data used in the simulations. Sections 4 and 5 present model results for the IN effect in the tropics and midlatitudes, respectively, and section 6 presents conclusions.

2. Experiment setup

a. *Model structure*

In this study, the Goddard Cumulus Ensemble (GCE) model, a CRM, is used to simulate clouds and precipitation. The model is detailed in Tao and Simpson (1993) and Tao et al. (2003a), who describe its development and main features. Its application to studies of precipitation processes and improving satellite retrievals can be found in Simpson and Tao (1993) and Tao (2003). The model is nonhydrostatic and anelastic. It has an option to change cloud microphysics from the three-class ice formulations of Lin et al. (1983) to that of Rutledge and Hobbs (1984) easily. It takes account of the absorption and scattering for solar radiation and the emission and absorption for infrared radiation. Its cloud–radiation interaction has been assessed (Tao et al. 1996). Subgrid-scale (turbulent) processes in the model are parameterized using a scheme based on Klemp and Wilhelmson (1978) and Soong and Ogura (1980). The effects of both dry and moist processes on the generation of subgrid-scale kinetic energy have been incorporated. The sedimentation of ice crystals was recently included in the GCE based on Heymsfield and Donner (1990) and Heymsfield and Iaquinta (2000) and was discussed in detail in Hong et al. (2004). All scalar variables (temperature, water vapor, and all hydrometeors) are calculated with a positive definite advection scheme (Smolarkiewicz and Grabowski 1990). Results from the positive definite advection scheme are in better agreement with observations for tropical cloud systems (Johnson et al. 2002).

The model in the present paper has the same structure as that in previous studies (e.g., Johnson et al. 2002; Xie et al. 2005; Xu et al. 2005; Zeng et al. 2007a) in which clouds are simulated under prescribed large-scale forcing. The default numerical experiment is three-dimensional (3D), using a 1-km horizontal resolution and a vertical resolution that ranges from 42.5 m at the

bottom to 1 km at the model top, which is at 22.5 km. The model uses a time step of 6 s and 256 × 256 × 41 grid points for integration. Seven vertical layers that extend to 0.01 hPa are added above the model top for radiative computations. The Rutledge and Hobbs (1984) scheme is used to represent the cloud microphysics with the modification described in Zeng et al. (2008). As was done by Wu et al. (1999) and Hong et al. (2004), the sedimentation of cloud ice (Starr and Cox 1985) is included to better model clouds in the upper troposphere. The interpolation of large-scale forcing data to model grid points is slightly modified so that the vertical integration of water forcing between the observations and the model is equal in magnitude. All other numerical experiments in the paper follow the default one except when specified.

b. Parameterization of the Bergeron process

The model uses the mixing ratios of cloud water, rainwater, cloud ice, snow, and graupel as prognostic variables to simulate hydrometeors. The IN concentration is introduced into the parameterization of the Bergeron (1935) process as an input factor (Zeng et al. 2008). Because IN concentration changes the cloud ice crystal concentration via heterogeneous nucleation and smaller crystals grow faster, it quickly changes the cloud ice crystal spectrum. Thus, Zeng et al. (2008) obtained the conversion rate of cloud ice to snow due to vapor deposition

$$\max[2a_1(3q_i - m_{I50}\rho^{-1}\mu N_i)m_{I50}^{a_2-1}, 0] \qquad (2.1)$$

and the conversion rate of cloud water to ice in the Bergeron process

$$\frac{2}{(a_2+1)(a_2+2)}[3a_2q_i + (1-a_2)m_{I50}\rho^{-1}\mu N_i]a_1m_{I50}^{a_2-1}, \qquad (2.2)$$

where N_i is the number concentration of active ice nuclei, q_i is the mixing ratio of cloud ice, a_1 and a_2 are the temperature-dependent parameters in the Bergeron process (Koenig 1971), ρ is the air density, $m_{I50} = 4.8 \times 10^{-7}$ g is the mass of an ice crystal 50 μm in diameter, and $\mu = 1.2$ is the ice particle enhancement factor due to a riming–splintering mechanism (Hallett and Mossop 1974) and other causes. Expression (2.1) degenerates into the original one (Hsie et al. 1980) when the ice crystal (or active IN) concentration is very small or $N_i \ll 3\rho q_i(\mu m_{I50})^{-1}$. Recently, Matsui et al. (2007) compared the modeled cloud properties with Tropical Rainfall Measuring Mission (TRMM) satellite observations and showed that the new scheme significantly improved the modeling of cloud properties, especially in the upper troposphere.

This new scheme is physically clear. Ice crystal concentration affects the conversion of cloud water to precipitating ice in the Bergeron process. When the concentration is much lower than cloud droplet concentration, for example, ice crystals can grow large through the process and further ice riming, resulting in the efficient conversion of cloud water to precipitating ice. In contrast, when the concentration is so high that it is close to cloud droplet concentration, ice crystals cannot grow large because they compete for available supercooled droplets and thus remain small. Expression (2.1) represents this role of ice crystal concentration in the Bergeron process because (2.1), given the mixing ratio of cloud ice q_i, decreases with increasing ice crystal concentration (or μN_i).

The number concentration of active natural ice nuclei N_i changes with air temperature T as[1] (Fletcher 1962)

$$N_i = n_0 \exp[\beta(T_0 - T)], \qquad (2.3)$$

where n_0 is typically about 10^{-8} cm^{-3} (with variations of several orders of magnitude), $\beta = 0.6$ (and can range from 0.4 to 0.8), and $T_0 = 273.16$ K. In this study, many CRM experiments are carried out that vary β and n_0 to show the effect of IN on clouds and radiation. For the sake of brevity, low, moderate, and high IN concentrations are defined as the cases with (β, n_0) = (0.4, 10^{-9} cm^{-3}), (0.5, 10^{-8} cm^{-3}), and (0.6, 10^{-6} cm^{-3}), respectively.[2]

3. Observational data from field campaigns

Nine field campaigns are chosen to provide large-scale forcing data for the CRM simulations. For each campaign case, three numerical experiments with low, moderate, and high IN concentrations are carried out to show the effect of IN on clouds and radiation. Ad-

[1] The IN expressions of Fletcher (1962) and Meyers et al. (1992) are equivalent in the mixed-phase region where the Bergeron process is active. Air is almost always saturated with respect to water in the mixed-phase region because water droplet number concentration is much higher than ice crystal number concentration (e.g., Korolev and Mazin 2003). Hence, the supersaturation with respect to ice is a function of temperature. Therefore, the two expressions are equivalent, where "equivalent" implies that the difference between the two expressions is smaller than the uncertainty of the parameters used to compute IN concentration.

[2] An ice crystal enhancement factor of $\mu = 1.2$ is used. Because μn_0 can be treated as one factor in (2.1) and (2.2), the sensitivity of cloud ensembles and their resulting radiation represents the sensitivity to n_0 (or μ) when μ (or n_0) is known.

TABLE 1. Field campaigns and their numerical experiments.

Field campaign	Geographic location	Starting date	Modeling days	Number of experiments
ARM-SGP-97	(37°N, 97°W)	18 Jun 1997	29	4
ARM-SGP-00		1 Mar 2000	20	4
ARM-SGP-02		25 May 2002	20	5
SCSMEX/NESA	(21°N, 117°E)	6 May 1998	44	3
SCSMEX/SESA	(5°N, 109°E)	1 May 1998	60	2
TWP-ICE	(12°S, 131°E)	19 Jan 2006	24	2
TOGA COARE	(2°S, 154°E)	1 Nov 1992	61	2
GATE	(9°N, 24°W)	1 Sep 1974	18	3
KWAJEX	(9°N, 167°E)	24 Jul 1999	52	2

ditional experiments with other IN concentrations may be carried out to show the extent of the IN effect. Table 1 lists the field campaigns discussed in the present paper and the numerical experiments with their number, starting date, and modeling days.

The nine campaigns, conducted in different geographic locations and seasons, provided different large-scale forcing to the CRM simulations. All of the CRM simulations with forcing are long, from 18 days to 2 months, so that the cloud ensembles are modeled properly. The campaigns and their numerical experiments are introduced next.

a. ARM-SGP

The Atmospheric Radiation Measurement (ARM) program set up the Southern Great Plains (SGP) site to observe clouds and precipitation for climate research (Ackerman and Stokes 2003). The site was centered at 36.6°N and 96.5°W. Three field campaigns at the site, referred to here as ARM-SGP-97, -00, and -02, were conducted in 1997, 2000, and 2002, respectively. The ARM observational data used are classified into two parts: forcing and evaluation data. Large-scale forcing data (i.e., vertical motion and horizontal advective tendencies of temperature and moisture) are derived using the variational analysis approach described in Zhang and Lin (1997) and Zhang et al. (2001). The values represent the mean over the ARM Cloud and Radiation Test Bed (CART) domain of 300×300 km^2 (Zhang et al. 2001). The surface fluxes are obtained from site-wide averages of observed fluxes from the ARM Energy Balance Bowen Ratio (EBBR) stations. Evaluation data include observed temperature and humidity as well as liquid and ice water contents. Temperature and humidity are observed every 3 h. Liquid and ice water contents are obtained from ARM Microbase products (Miller et al. 2003).

The ARM-SGP-97 forcing data have been used to simulate clouds and precipitation for model intercomparison (e.g., Xu et al. 2002, Xie et al. 2002; Khairoutdinov and Randall 2003). Using these data, three numerical experiments with low, moderate, and high IN concentrations are performed here. One more experiment with a very low IN concentration is also made using $\beta = 0.3$ and $n_0 = 5 \times 10^{-10}$ cm^{-3}. All four experiments start at 2330 UTC 18 June 1997 and last for 29 days.

The ARM-SGP-00 forcing data have been used to simulate clouds in comparison with observations (e.g., Xie et al. 2005; Xu et al. 2005; Zeng et al. 2007a; Wu et al. 2008). Using these data, four numerical experiments are conducted with very low, low, moderate, and high IN concentrations, respectively. All the experiments start at 1730 UTC 1 March 2000 and last for 20 days.

The ARM-SGP-02 forcing data have been used to study clouds and the effect of surface fluxes on clouds (Zeng et al. 2007a). Here, four numerical experiments are done following those for the ARM-SGP-00 case. In addition, one more experiment is made using $\beta = 0.45$ and $n_0 = 4 \times 10^{-9}$ cm^{-3}. All five experiments start at 2030 UTC 25 May 2002 and last for 20 days.

The ARM-SGP-97 and -02 numerical experiments simulate summertime clouds that are associated with continental convection. In contrast, the ARM-SGP-00 experiments model springtime clouds that are embedded in fronts, cyclogenesis, and upper-level trough systems.

b. TOGA COARE

The Tropical Ocean Global Atmosphere (TOGA) Coupled Ocean–Atmosphere Response Experiment (COARE) took place from 1 November 1992 to 28 February 1993 (Webster and Lukas 1992). It was centered at 2°S and 154°E. The large-scale forcing data from the experiment have been widely used in CRM simulations (e.g., Wu et al. 1998; Petch and Gray 2001; Wu and Moncrieff 2001). The data, derived by a group at Colorado State University (CSU) with a humidity

correction; (Ciesielski et al. 2003), are used to conduct two numerical experiments. The two experiments use the moderate and high IN concentrations, respectively. They start at 0000 UTC 1 November 1992 and last for 61 days.

c. SCSMEX

The South China Sea Monsoon Experiment (SCSMEX), part of the field campaigns in support of the TRMM (Simpson et al. 1988), was conducted over two sounding polygons in May–June 1998. The experiment addressed the key processes for the onset and evolution of the summer monsoon over Southeast Asia and southern China (e.g., Lau et al. 2000; Johnson and Ciesielski 2002). The Northern Enhanced Sounding Array (NESA) polygon was centered at 21°N and 117°E; the Southern Enhanced Sounding Array (SESA) polygon was centered at 5°N and 109°E.

The SCSMEX/NESA forcing data have been used to model clouds in comparison with observations (Tao et al. 2003b; Zhou et al. 2007; Zeng et al. 2008). Using the data obtained from a variational analysis approach (Zhang and Lin 1997; Zhang et al. 2001), three numerical experiments are carried out to address the effect of IN on radiation. Two of the three experiments use the moderate and high IN concentration; the other uses $n_0 = 10^{-5}$ cm^{-3} and $\beta = 0.7$ (very high IN concentration). All the experiments start at 0600 UTC 6 May 1998 and last for 44 days.

The CSU forcing data for SCSMEX/SESA are used to conduct two experiments: moderate and high IN concentration, respectively. They start at 0000 UTC 1 May 1998 and last for 60 days.

d. KWAJEX

The Kwajalein Experiment (KWAJEX), another TRMM field campaign, took place around Kwajalein Atoll from 23 July through 15 September 1999. It was centered at 8.8°N and 167.4°E. Forcing data from the experiment have been used in CRM simulations (Blossey et al. 2007; Zeng et al. 2008). Variational analysis data are used to perform two experiments: moderate and high IN concentration, respectively. The experiments start at 0600 UTC 24 July 1999 and last for 52 days.

e. GATE

The Global Atmospheric Research Program's (GARP's) Atlantic Tropical Experiment (GATE) was conducted in the summer of 1974. It was centered at 9°N and 24°W. Its forcing data have been used in many CRM simulations (Sui et al. 1994; Xu and Randall 1996; Grabowski et al. 1999; Phillips and Donner 2006). Using the forcing data from Ooyama (1987), two experiments are done here with moderate and high IN concentrations, respectively. In addition, one more experiment with very high IN concentration is done, using $\beta = 0.7$ and $n_0 = 10^{-5}$ cm^{-3}. All the experiments start at 0000 UTC 1 September 1974 and last for 18 days.

f. TWP-ICE

The Tropical Warm Pool–International Cloud Experiment (TWP-ICE) was conducted in the area around Darwin, Australia, in January and February of 2006. It was centered at 12°N and 131°E. The corresponding large-scale forcing data derived from variational analysis are used to conduct two numerical experiments: moderate and high IN concentration, respectively. They start at 1500 UTC 19 January 2006 and last for 24 days.

All of the numerical experiments are grouped into tropical and midlatitudinal. The tropical experiments include those based on data from the GATE, TOGA COARE, SCSMEX/NESA, SCSMEX/SESA, KWAJEX, and TWP-ICE field campaigns, and the midlatitudinal use the data from the ARM-SGP field campaigns in the summer of 1997, spring of 2000, and summer of 2002. In the following two sections, the two groups of experiments are compared to show the differing effects of IN in the midlatitudes and tropics in turn.

4. Numerical experiments on tropical clouds

With the aid of CRM simulations, this section explores the effect of IN on radiation in the tropics, beginning with the effect of IN on clouds and precipitation. It then analyzes the IN effect on the precipitation efficiency of clouds and finally on radiation.

a. Effect of IN on precipitation

Six sets of numerical experiments are carried out to simulate clouds over six tropical locations, respectively. In each set of experiments, low, moderate, and high IN concentrations are usually used to model the effect of IN on clouds (see Table 1). The two GATE experiments, for example, use moderate and high IN concentrations, respectively. They start on 0000 UTC 1 September 1974 and last for 18 days. The modeled surface precipitation rates are displayed against time in Fig. 1. These modeled rates are close to the observed. The mean precipitation rate decreases from 12.2 to 11.8 mm day^{-1} as the IN concentration increases from moderate

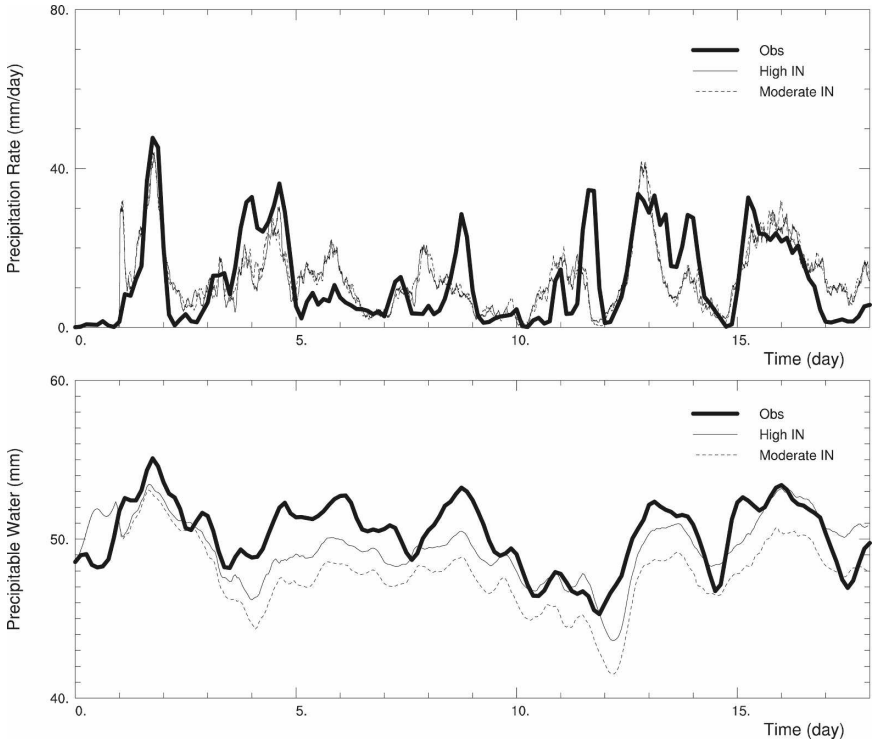

FIG. 1. Time series of (top) surface precipitation rate and (bottom) precipitable water in the GATE numerical experiments. Thick lines represent the observations. Thin solid and dashed lines represent the modeling results with high and moderate IN concentration, respectively.

to high. It approaches the observed of 11.4 mm day^{-1} when the high IN concentration is used.

Figure 1 also displays the modeled precipitable water versus time in the two experiments. The precipitable water increases with increasing IN concentration and approaches the observed when the high IN concentration is used. The sensitivity of precipitable water to IN concentration is associated with the sensitivity of surface precipitation rate via water conservation. Consider a slight precipitation bias on a long time scale. It can eventually accumulate into a considerable bias in precipitable water. In other words, a slight decrease in surface precipitation due to increasing IN concentration can bring about a significant increase in precipitable water.

b. *Effect of IN on clouds*

The sensitivity of precipitable water to IN concentration is associated with the effect of IN on ice species. Figures 2 and 3 display the time–pressure cross sections of cloud ice, snow, and graupel in the two GATE experiments for moderate and high IN concentrations, respectively. As shown in the figures, the high IN concentration brings about more cloud ice and snow but less graupel than the moderate IN concentration. This repartitioning of ice species due to IN variation explains the effect of IN on precipitable water from another perspective. Because the fall speed of cloud ice and snow is smaller than that of graupel, cloud ice and snow stay aloft longer than graupel. Thus, more cloud ice and snow lead to more precipitable water via sublimation. Hence, the effect of IN on ice species shown is consistent with that of IN on precipitable water shown in Fig. 1.

Similar effects of IN on ice species and precipitable water are found in all the other tropical experiments (figures omitted). In summary, an increase in IN concentration leads to a decrease in surface precipitation and thus an increase in precipitable water via ice species partitioning. Next, the precipitation efficiency of clouds is used to measure the effect of IN on ice species partitioning quantitatively.

c. *Effect of IN on the bulk precipitation efficiency of clouds*

The precipitation efficiency of clouds has had different definitions in different studies (e.g., Rogers and Yau 1989; Tao et al. 2004). Braham (1952) defined PE

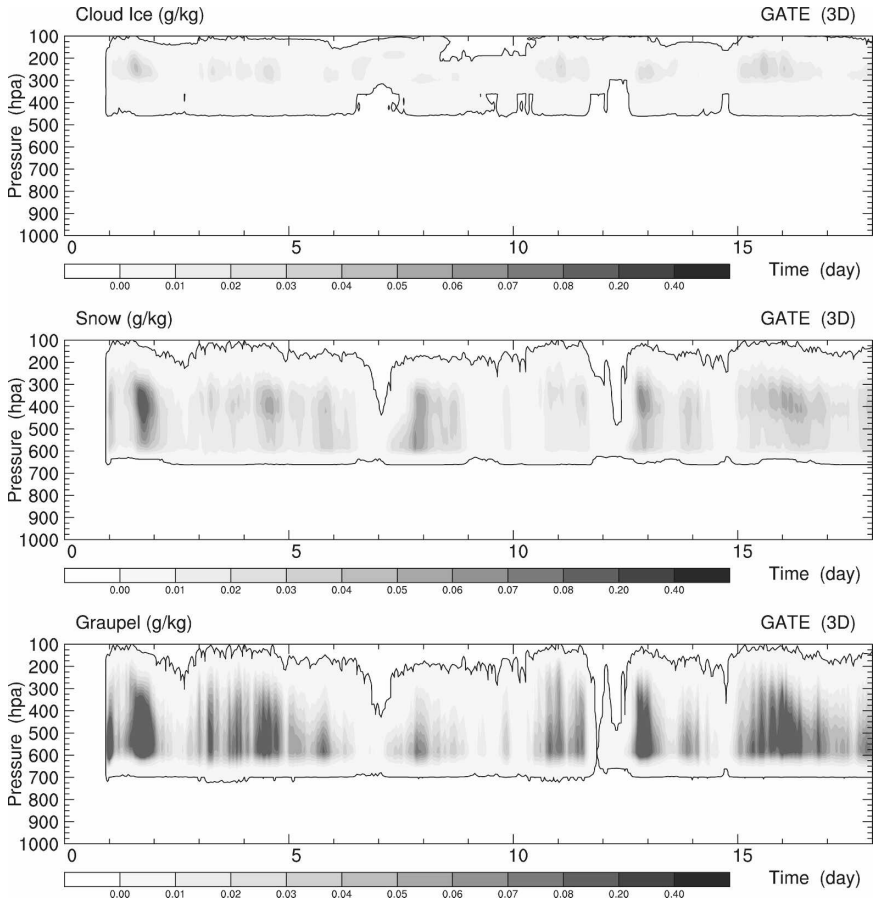

FIG. 2. Time–pressure cross sections of the mixing ratios of (top) cloud ice, (middle) snow, and (bottom) graupel for the GATE experiment with moderate IN concentration.

as the ratio of the mass of rain reaching the ground to the mass of vapor entering the cloud. To measure the conversion of water vapor to precipitation in bulk, the present paper revises the Braham definition as the ratio of the surface precipitation rate to the maximum upward mass flux of airborne water (or all nonprecipitating water). Figure 4 displays the bulk PE of clouds against IN concentration for the tropical experiments, where the IN concentration is calculated with (2.3) at −10°C. Because the mixed-phase region is not commonly observed once temperatures become colder than −20°C (e.g., Pruppacher and Klett 1997), the IN concentration at −10°C can be used as an index to represent the concentration of active IN in clouds. As shown in Fig. 4, the PE decreases with increasing IN concentration in the tropics.

The effect of IN on the PE is physically clear. Inside convective clouds with coexisting supercooled droplets and ice crystals, snow and graupel increase mainly via vapor deposition and riming. Because graupel has a large fall speed and thus collects supercooled droplets efficiently, it can grow quickly when supercooled droplets are abundant. Hence, the bulk PE increases with increasing graupel and decreasing snow, and therefore the effect of IN on the bulk PE is attributed to the effect of IN on ice species partitioning as shown in Figs. 2 and 3.

d. *Effect of IN on upper tropospheric cloud ice*

Supercooled droplets in the middle troposphere can freeze and be transported into the upper troposphere. Thus, the precipitation processes in the middle troposphere can affect upper-tropospheric (UT) ice. Figure 5 displays the horizontally averaged cloud ice content above 7.4 km versus the IN concentration at −10°C in the tropical experiments. The content increases with increasing IN concentration, especially in the SCSMEX/NESA case. This effect of IN on UT ice is associated with the effect of IN on PE. Based on UT water balance and the definition of PE, UT cloud ice content depends on PE and the upward water mass flux in the lower troposphere. Suppose that the upward wa-

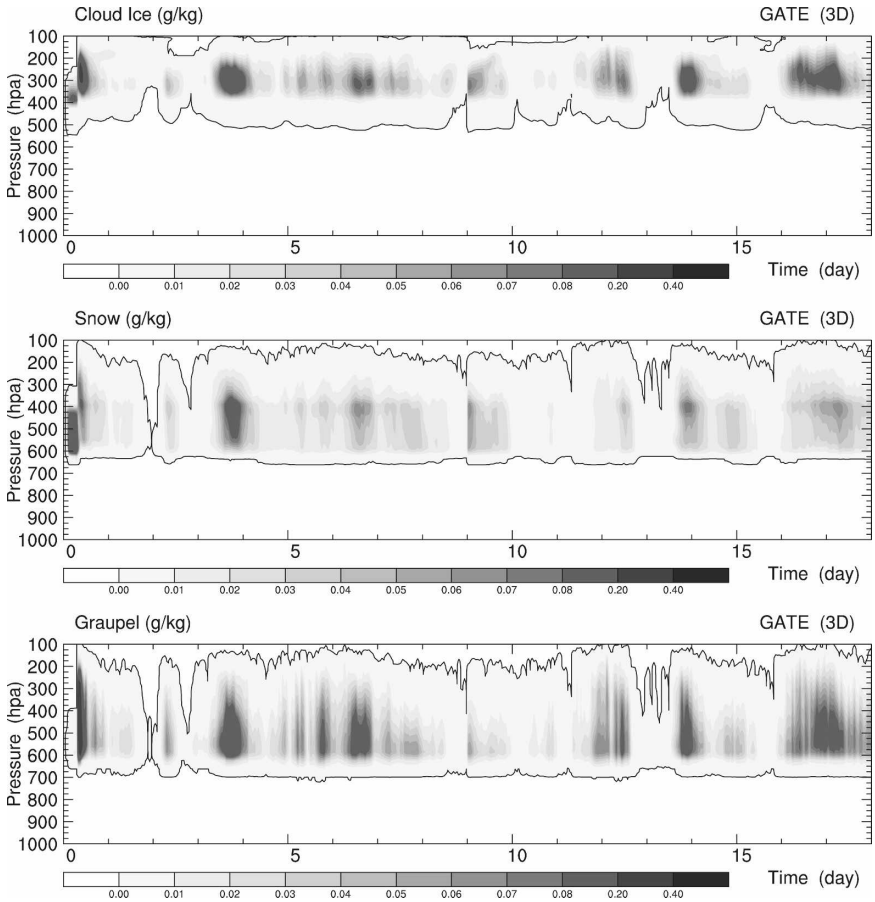

FIG. 3. As in Fig. 2, but for high IN concentration.

ter mass flux changes little with IN concentration. In that case, UT cloud ice increases with decreasing PE, which can lead to the sensitivity of UT cloud ice to IN concentration.

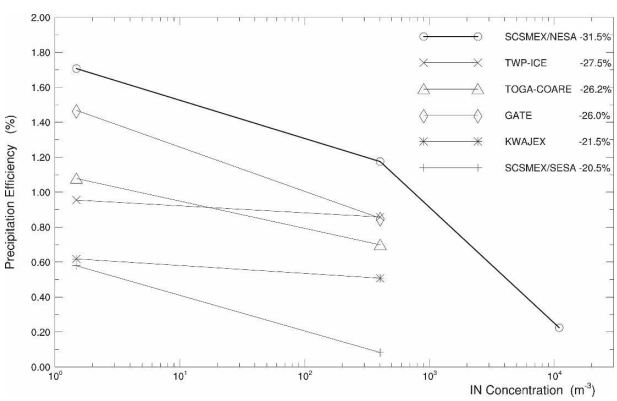

FIG. 4. Bulk precipitation efficiency of clouds vs IN concentration in the tropical experiments. The vertical axis represents the PE minus a value shown in the upper right corner; the horizontal axis represents the IN concentration at −10°C.

In fact, the upward water mass flux is not sensitive to IN concentration. In the two GATE experiments with moderate and high IN concentration, for example, the upward water mass fluxes at 831 hPa are 1.85 and 1.84 mm h^{-1} and the bulk PE is 27.5% and 26.9%, respectively. Other evidence shows that IN affects cloud dy-

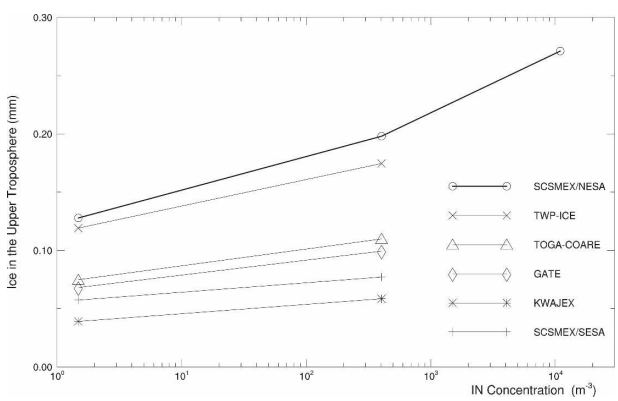

FIG. 5. Cloud ice content above 7.4 km vs the IN concentration at −10°C in the tropical experiments.

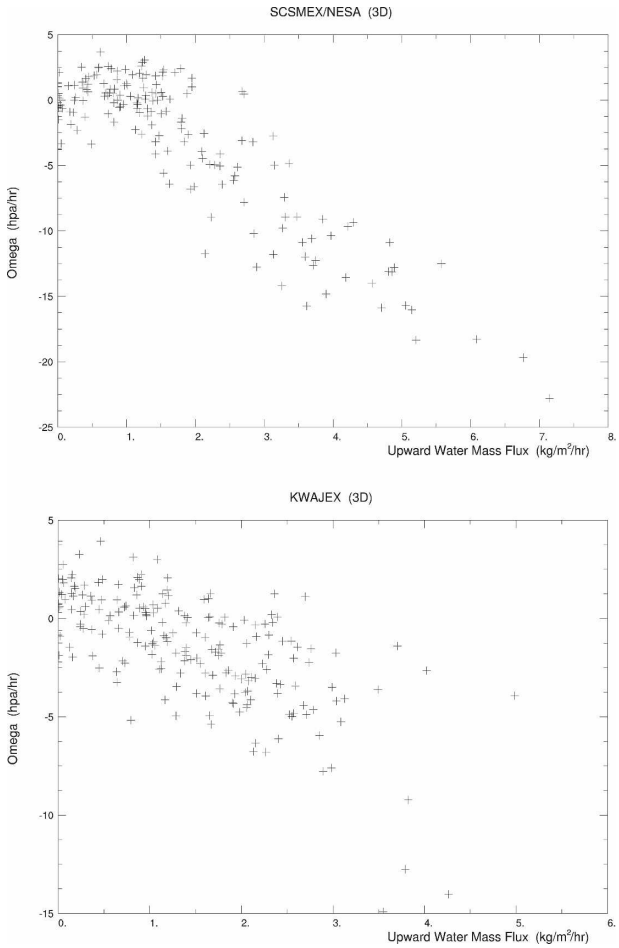

FIG. 6. Upward water mass flux at 850 hPa vs the large-scale upward velocity (top) at 450 hPa in the SCSMEX/NESA experiment and (bottom) at 650 hPa in the KWAJEX experiment with high IN concentration.

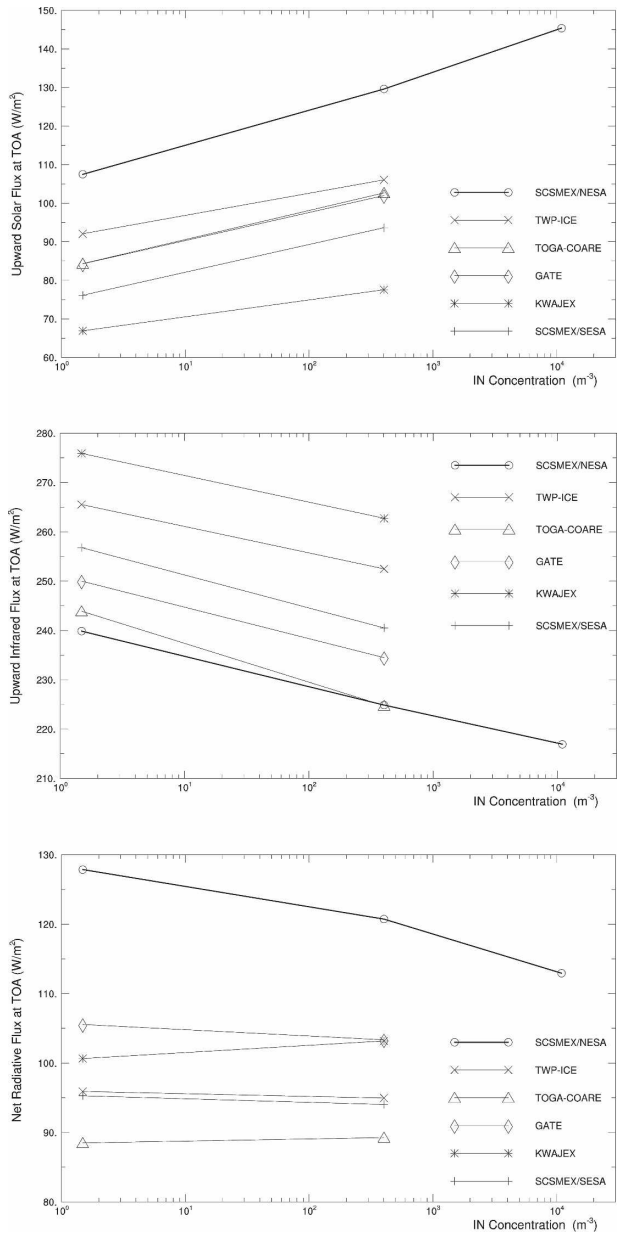

FIG. 7. (top) Upward solar, (middle) infrared, and (bottom) downward net radiative flux at the TOA vs the IN concentration (at −10°C) in the tropical experiments.

namics slightly. The probability density functions (PDFs) of vertical velocity in the two GATE experiments, for example, resemble each other (figure omitted), which shows that the PDF is not sensitive to IN concentration. Hence, IN changes cloud microphysics more than cloud dynamics.

The upward water mass flux in the lower troposphere is determined by the large-scale upward motion. Two examples include the SCSMEX/NESA and KWAJEX experiments with high IN concentration. Figure 6 displays the upward water mass flux at 850 hPa against large-scale upward motion. Because the mean large-scale upward velocity is largest at 450 and 650 hPa in SCSMEX/NESA and KWAJEX, respectively, the horizontal axis of Fig. 6 represents the large-scale upward velocity at 450 hPa in SCSMEX/NESA and 650 hPa in KWAJEX. The figure shows that the upward flux, when larger than 0.5 kg m^{-2} h^{-1}, is positively correlated with large-scale upward motion. A positive correlation between the two variables also exists in the other tropical experiments (figures omitted), which indicates that the large-scale upward motion in the middle troposphere determines the upward water mass flux in the lower troposphere.

The correlation between the upward water mass flux and the large-scale upward motion is physically clear. Large-scale upward motion controls the number of convective updraft cores in the middle troposphere, and

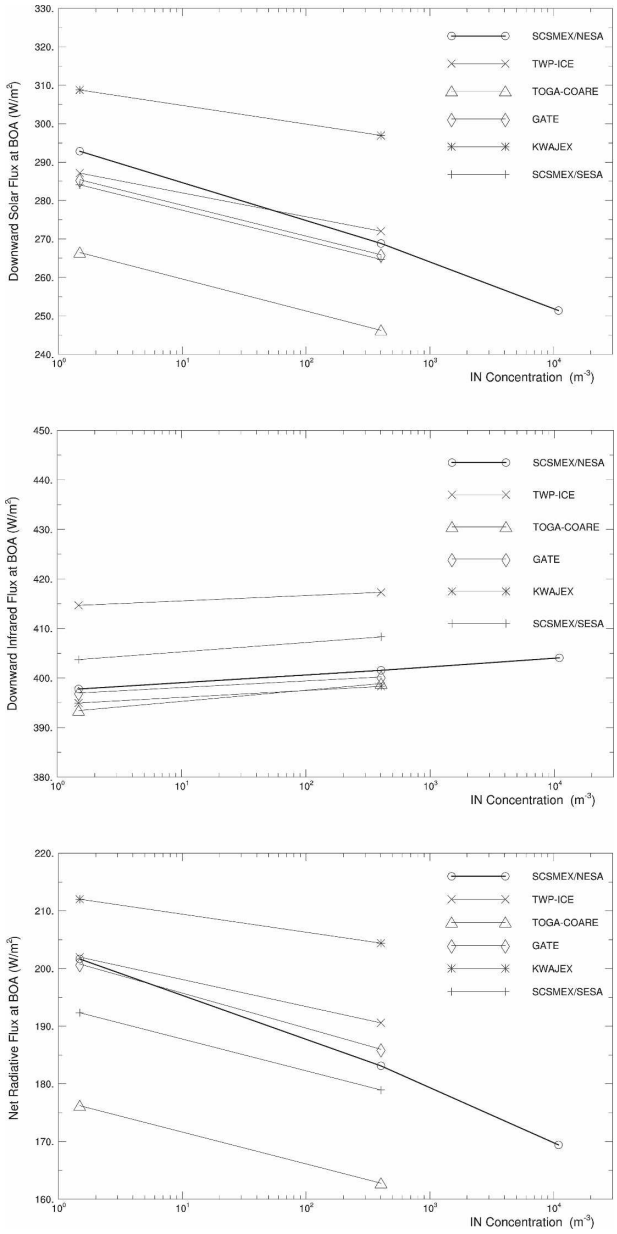

FIG. 8. As in Fig. 7, but at the bottom of the atmosphere.

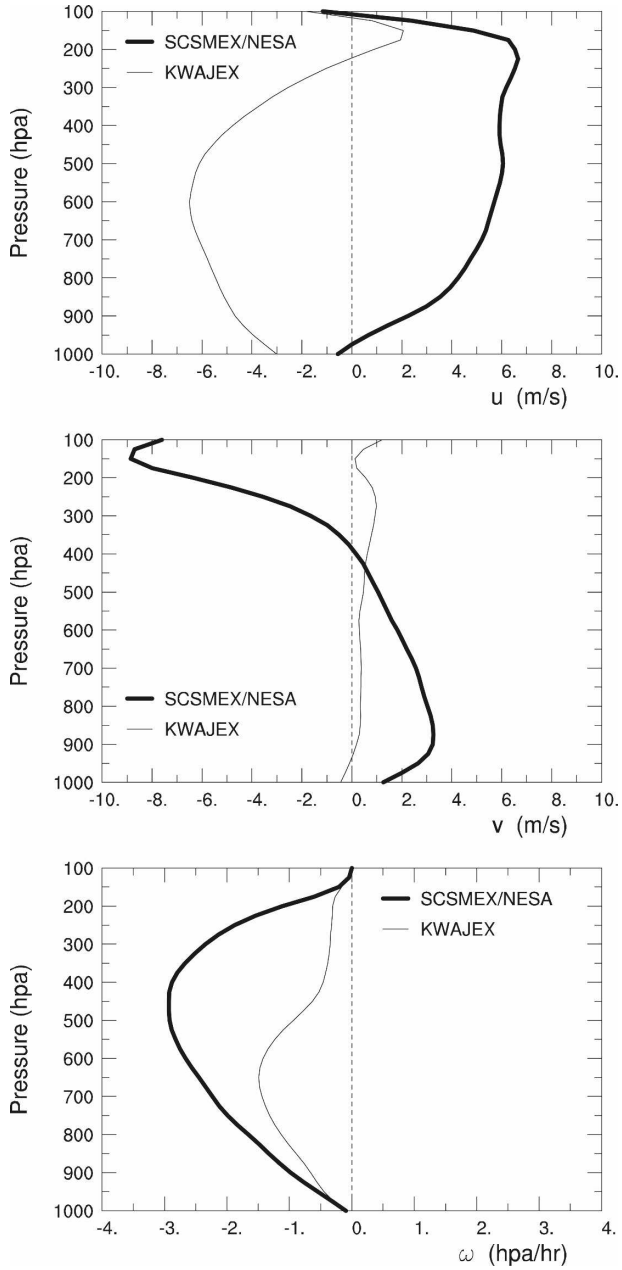

FIG. 9. Vertical profiles of large-scale (top) longitudinal, (middle) meridional, and (bottom) vertical wind in the SCSMEX/NESA (thick line) and KWAJEX (thin line) cases.

then the updraft cores bring about convective downdrafts in the mature and dissipating stages (Byers and Braham 1948). Because of mass conservation in the planetary boundary layer, large-scale upward motion in the middle troposphere determines the upward water mass flux in the lower troposphere via convective downdrafts.

e. Indirect effect of IN on radiation

IN affect UT cloud ice, which in turn modulates solar and infrared radiation. Figure 7 displays the upward solar and infrared fluxes at the TOA versus the IN concentration at −10°C. The upward solar flux increases with increasing IN concentration, whereas the infrared one decreases. Because IN modulates the upward solar and infrared fluxes oppositely, the effect of IN on the net radiative flux at the TOA varies from one case to another. Figure 7 displays the downward net radiative fluxes at the TOA versus the IN concentration. The net flux decreases considerably

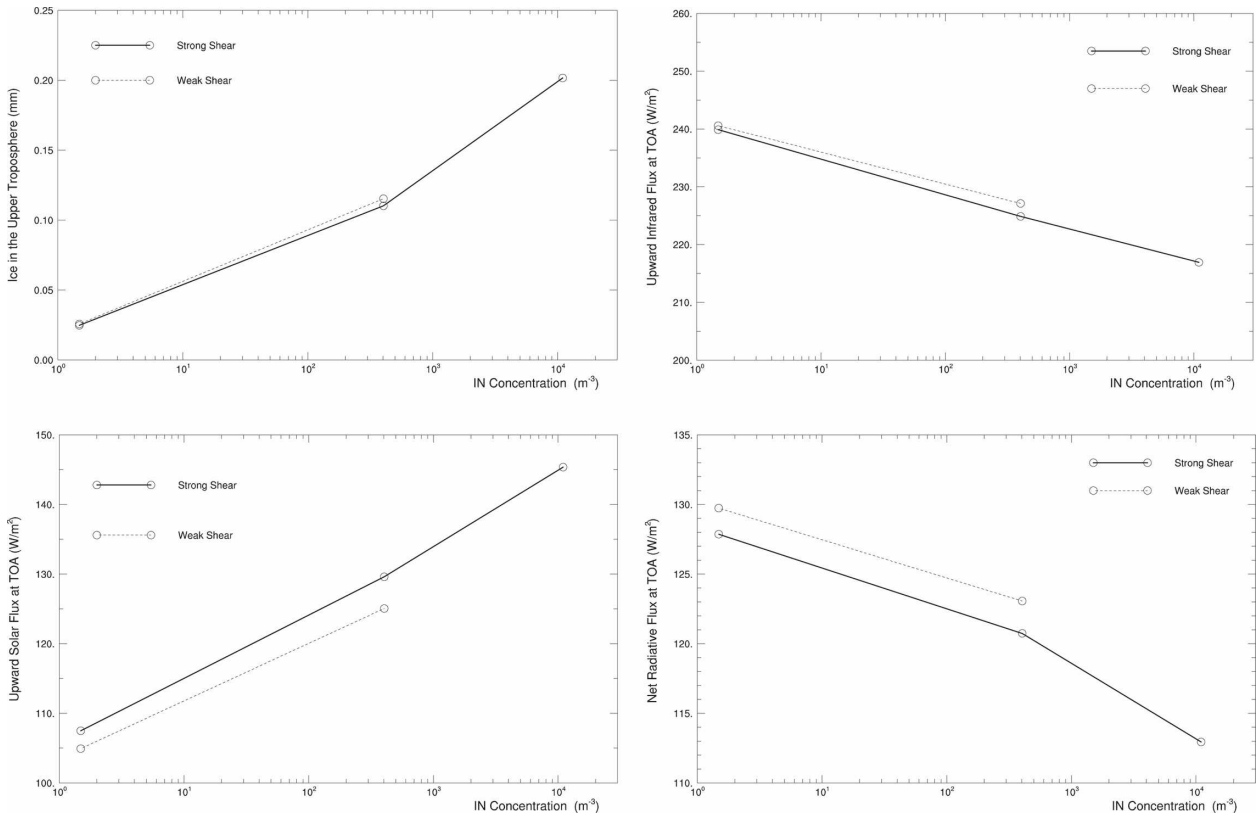

FIG. 10. (top left) UT cloud ice content and (top right) upward infrared, (bottom left) solar, and (bottom right) downward net radiative flux at the TOA vs the IN concentration at −10°C. Solid and dashed lines represent the SCSMEX/NESA modeling results when the vertical wind shear is strong (or original) and weak (or decreased), respectively.

with IN concentration in SCSMEX/NESA but only slightly in GATE, TWP-ICE and SCSMEX/SESA. The net flux increases slightly in KWAJEX and TOGA COARE.

The effect of IN on the radiative fluxes at the TOA is associated with the effect of IN on UT ice. High cirrus reflect solar radiation back into space while emitting infrared radiation to space at low cloud top temperatures. Thus, an increase in UT cirrus leads to an increase in solar reflection and a decrease in upward infrared emission, which leads to opposing effects of IN on the upward solar and infrared fluxes at the TOA.

Figure 8 displays the downward solar, infrared, and net radiative fluxes at the bottom of the atmosphere (BOA) against the IN concentration at −10°C. With increasing IN concentration, the downward solar flux decreases with increasing IN concentration whereas the infrared one increases. In spite of the opposite response of the fluxes to IN concentration, the net radiative flux at the BOA still decreases with increasing IN concentration.

The effect of IN on the radiative fluxes at the BOA is associated with the effect of IN on UT ice, too. High cirrus reflect solar radiation and thus weaken the radiation that reaches the ground. Simultaneously, high cirrus absorb the upward infrared radiation emitted by the ground and the air below and then re-emit infrared radiation back to the ground. Hence, with increasing UT cloud ice, the downward solar flux at the BOA decreases whereas the infrared one increases, which leads to opposing effects on the solar and infrared fluxes at the BOA.

f. Effect of IN effect on radiation via vertical wind shear

Vertical wind shear, especially in the upper troposphere, can change the effect of IN on radiation via UT cirrus. Figure 7 shows that the upward solar and infrared fluxes at the TOA in SCSMEX/NESA are the largest and smallest, respectively, of all the tropical cases. In contrast, the solar and infrared fluxes in KWAJEX are the smallest and largest, respectively. Thus, the SCSMEX/NESA and KWAJEX experiments are chosen as an example to show the effect of vertical wind shear on radiation.

Figure 9 displays the three components of the mean

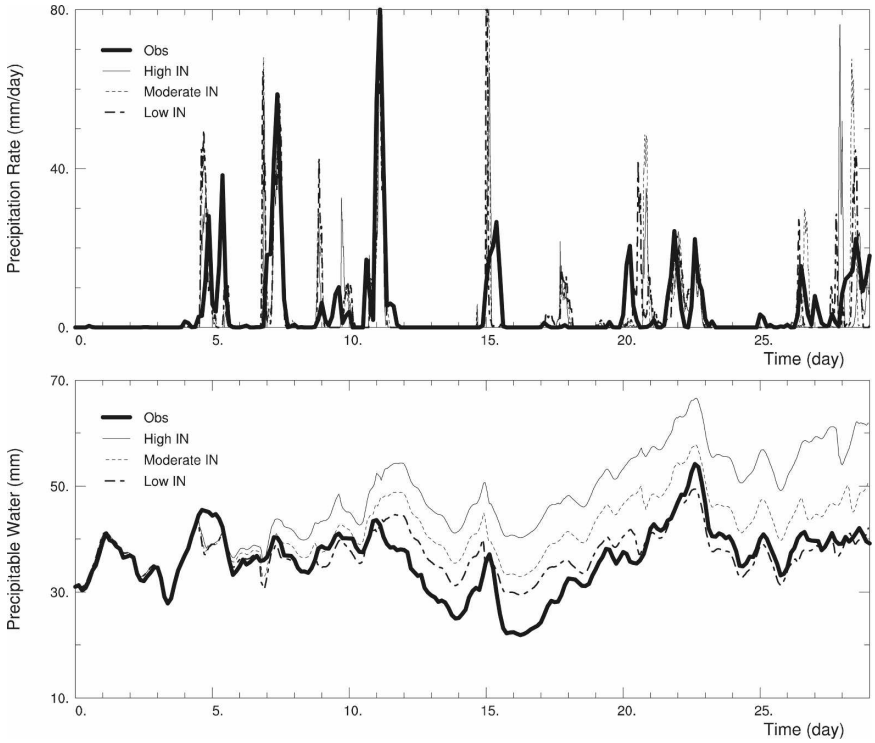

FIG. 11. Time series of (top) surface precipitation rate and (bottom) precipitable water for the ARM-SGP-97 case. Thick lines represent the observations. The thin solid, dashed, and thick dashed lines represent the modeling results for the high, moderate, and low IN concentrations, respectively.

large-scale velocity against pressure in the two cases. First, the large-scale upward motion in SCSMEX/NESA is much stronger than in KWAJEX, and the height for the strongest upward motion is higher. Hence, convective clouds in SCSMEX/NESA are stronger and transport cloud ice higher than those in KWAJEX, which leads to the difference in UT ice content and TOA radiative fluxes between the two cases.

Second, the UT vertical wind shear in SCSMEX/NESA, especially between 150 and 350 hPa, is stronger than in KWAJEX. Because vertical wind shear impacts cloud ensembles (Liu and Moncrieff 2001; Cohen and Craig 2006), the two SCSMEX/NESA experiments with moderate and high IN concentrations are redone to explore the effect of vertical wind shear on radiation. The two new experiments decrease the large-scale horizontal wind by a prescribed factor: the ratio of air pressure to its surface value. Their results as well as those of the two old experiments (i.e., cloud ice content above 7.4 km; upward solar, infrared, and downward net radiative fluxes at the TOA) are displayed in Fig. 10. As vertical wind shear increases, the UT cloud ice content decreases slightly. Consequently, the upward infrared flux at the TOA decreases slightly whereas the solar flux increases considerably. As a result, the net radiative flux at the TOA increases considerably.

The effect of vertical wind shear on radiation is understandable. Consider a high cirrus cloud detrained from convective cores. The cloud is so thick that it is opaque for both solar and infrared radiation. Based on the energy balance in the tropics (Riehl and Malkus 1958), it can be inferred that the net radiative flux at the TOA over this cloud is smaller than the regular one. Thus, with increasing vertical wind shear, the cloud is extended horizontally. As a result, the solar reflection of the cloud increases considerably and therefore the upward infrared flux at the TOA decreases.

5. Numerical experiments on midlatitudinal clouds

Owing to geostrophic balance, large meridional gradient of temperature brings about a strong thermal wind, which in turn brings about strong vertical wind shear in the middle latitudes. Because vertical wind shear and atmospheric stability affect radiation via clouds and are quite different between the midlatitudes and tropics, three sets of ARM-SGP numerical experiments (see Table 1) are conducted to show the effect of IN on radiation in the middle latitudes.

a. Numerical experiments on summertime clouds

Three numerical experiments with low, moderate, and high IN concentrations are carried out using

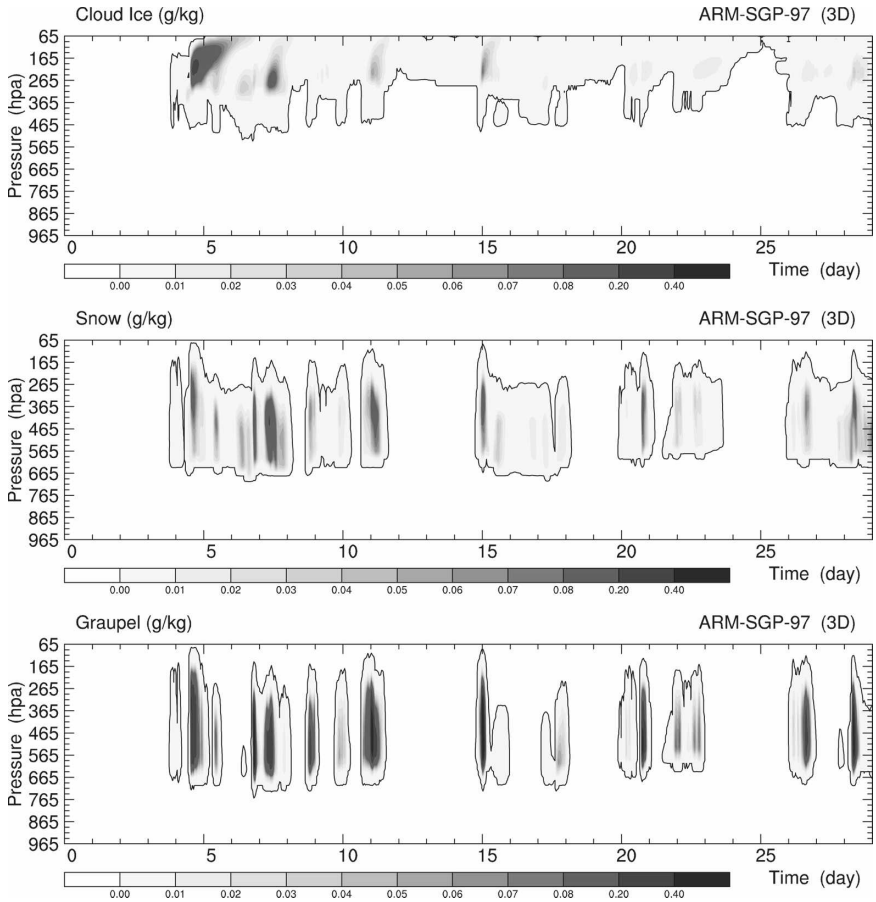

FIG. 12. Time–pressure cross sections of the mixing ratios of (top) cloud ice, (middle) snow, and (bottom) graupel for the ARM-SGP-97 experiment with low IN concentration.

ARM-SGP-97 large-scale forcing data. The modeled surface precipitation rate is shown against time in Fig. 11. The mean precipitation rate is 4.2, 3.9, and 3.5 mm day^{-1} for low, moderate, and high IN concentrations, respectively. Hence, the precipitation rate decreases with IN concentration and approaches the observed value of 4.3 mm day^{-1} when the low IN concentration is used. The modeled precipitable water is also shown versus time in Fig. 11. It approaches the observations when the low IN concentration is used.

Figures 12 and 13 show the time–pressure cross sections of simulated ice species for low and high IN concentrations, respectively. The high IN concentration brings about more cloud ice and snow but less graupel than the low one. This effect of IN on ice species segregation is similar to that in the tropics. To support this conclusion, three ARM-SGP-02 numerical experiments with low, moderate, and high IN concentrations were also conducted on summertime clouds. Those results resembled the ARM-SGP-97 experiments (figures omitted) with regard to the IN effect.

In these experiments on summertime clouds, surface precipitation decreases and precipitable water increases with increasing IN concentration, which resembles the tropical experiments. However, modeled precipitable water and precipitation rate are closer to observed values at the low IN concentration in the middle latitudes but at the high one in the tropics. Because sufficient IN observations are lacking, the present simulations can be treated as a proxy for ice particle concentration (or active IN concentration times the ice crystal enhancement factor). The modeling biases in relation to IN concentration suggest that ice particle concentrations in midlatitudinal clouds are less than in tropical clouds. This conclusion is consistent with previous observations because no ice particles, for example, were found in some midlatitudinal continental cumulus clouds with a cloud top temperature of about −20°C (Paluch 1979).

b. Numerical experiments on springtime clouds

Three numerical experiments with low, moderate, and high IN concentration are performed for spring-

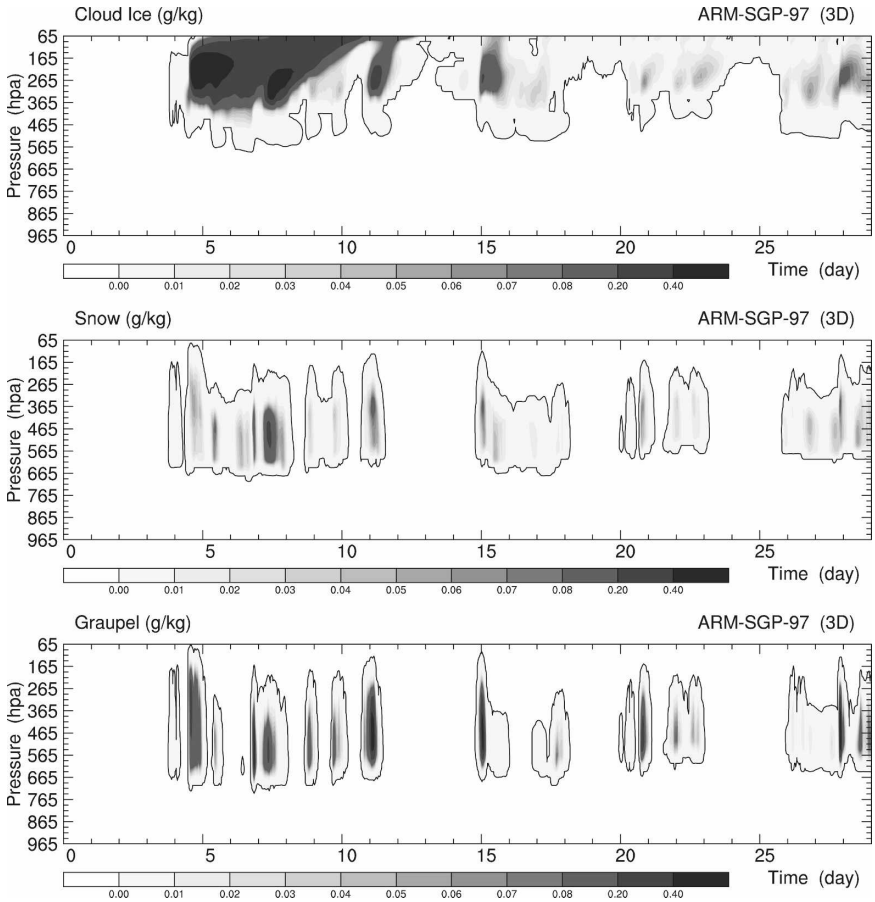

FIG. 13. As in Fig. 12, but for high IN concentration.

time clouds in midlatitudes using ARM-SGP-00 large-scale forcing data. Figure 14 displays their surface precipitation rates versus time. The mean precipitation rates are 4.0, 3.7, and 3.4 mm day^{-1} for low, moderate, and high IN concentrations, respectively. Thus, the precipitation rate decreases with IN concentration and approaches the observed value of 4.1 mm day^{-1} when the low IN concentration is used. Figure 14 also displays the modeled precipitable water versus time. The precipitable water decreases with decreasing IN concentration and approaches the observations when the low IN concentration is used.

To further illustrate the closeness between observations and the modeling results with a low IN concentration, Fig. 15 displays the time–pressure cross sections of ice water content from the two experiments as well as the observed. The figure clearly shows that UT ice water content decreases with decreasing IN concentration and the modeled ice content is close to the observed when the low IN concentration is used, especially in the upper troposphere. In summary, the effects of IN on precipitable water, precipitation rate, and UT ice water content in springtime clouds mimic those in summertime clouds, and the modeled results approach the observed when a low IN concentration is used.

c. *Effect of IN on UT cloud ice in middle latitudes*

Figure 16 displays the cloud ice content above 7.4 km versus the IN concentration at −10°C for all of the ARM-SGP numerical experiments. The content increases with IN concentration. To understand the effect of IN on UT ice, Fig. 17 shows the bulk PE of clouds versus the IN concentration at −10°C in the ARM-SGP experiments. The PE decreases significantly with increasing IN concentration, which implies that IN have a strong effect on UT ice in middle latitudes.

The effect of IN on UT ice, as shown in Fig. 16, is stronger in spring (or ARM-SGP-00) than in summer (or ARM-SGP-97 and -02). To understand this difference in the two seasons, Fig. 18 displays the mean mixing ratios of cloud water, rainwater, cloud ice, snow, and graupel against pressure in the ARM-SGP-00 and -97 experiments with low IN concentration. In contrast

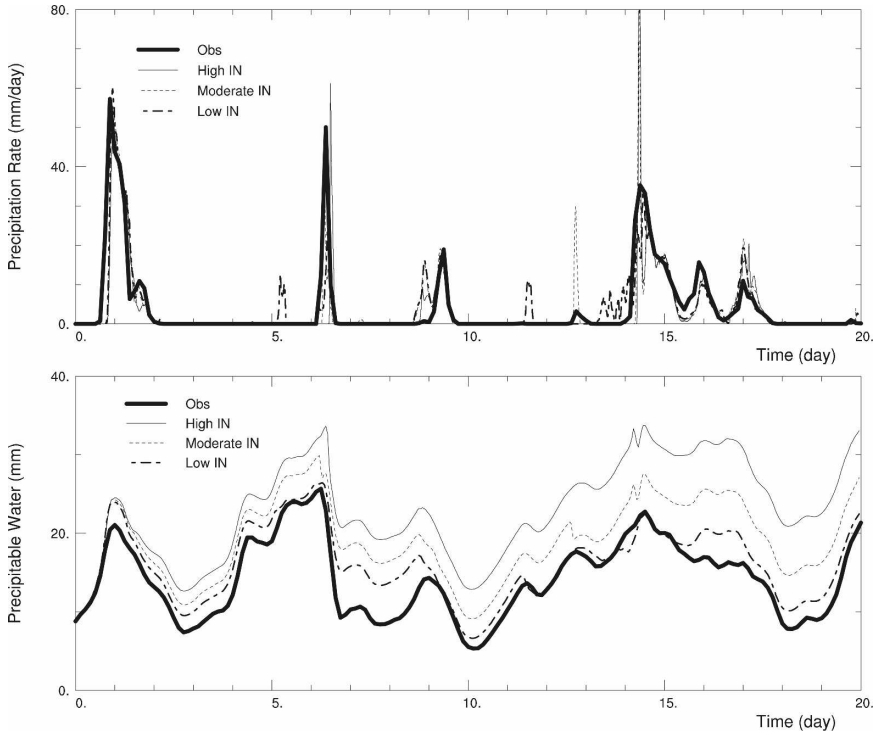

FIG. 14. As in Fig. 11, but for the ARM-SGP-00 case.

to ARM-SGP-97 clouds, the clouds in 2000 have more snow than graupel. Hence, the Bergeron process is more important than graupel riming in spring precipitation. Because the Bergeron process is sensitive to ice particle concentration, UT cloud ice is also sensitive to IN concentration in spring.

In contrast to the springtime clouds, the ARM-SGP-97 clouds have more graupel than snow (see Fig. 18). Hence, graupel riming is more important than the Bergeron process in summer precipitation. Because graupel riming is proportional to the graupel and supercooled water contents, its sensitivity to IN concentration is weaker than that of the Bergeron process. As a result, the effect of IN on UT cloud ice is weaker in summer than in spring.

d. IN effect versus latitude

Figures 16 and 17 display the effects of IN on UT cloud ice and PE at different latitudes. The IN effects are much larger in the middle latitudes than in the tropics, which is associated with the differences in ice species. Figure 18 exhibits the mean mixing ratios of ice species against pressure in the GATE experiment with high IN concentration. It also displays the same variables from an ARM-SGP-97 experiment for comparison. Because GATE clouds have more cloud and rainwater than ARM-SGP-97 ones, graupel riming contributes more to precipitation in the tropics than in midlatitudes. Hence, the effect of IN on UT cloud ice is weaker in the tropics than in midlatitudes.

e. Effect of IN on radiation in middle latitudes

Figure 19 displays the upward solar and infrared fluxes at the TOA versus the IN concentration at $-10°C$ for all of the ARM-SGP experiments. The upward solar flux decreases significantly with decreasing IN concentration whereas the infrared one increases. In addition, the modeled ARM-SGP-97, -00, and -02 upward infrared fluxes for the low IN concentration are close to the observed of 262.1, 228.4, and 252.8 W m^{-2}, respectively, which supports the previous conclusion that the model results at low IN concentration are close to observations.

Figure 19 also displays the radiative fluxes at the TOA for some tropical experiments for comparison. The effect of IN on the fluxes is much stronger in midlatitudes than in the tropics. This effect versus latitude is associated with the effect of IN on UT cloud ice as shown in Fig. 16.

The lower part of Fig. 19 shows the downward net radiative flux at the TOA versus IN concentration for the ARM-SGP numerical experiments as well as some

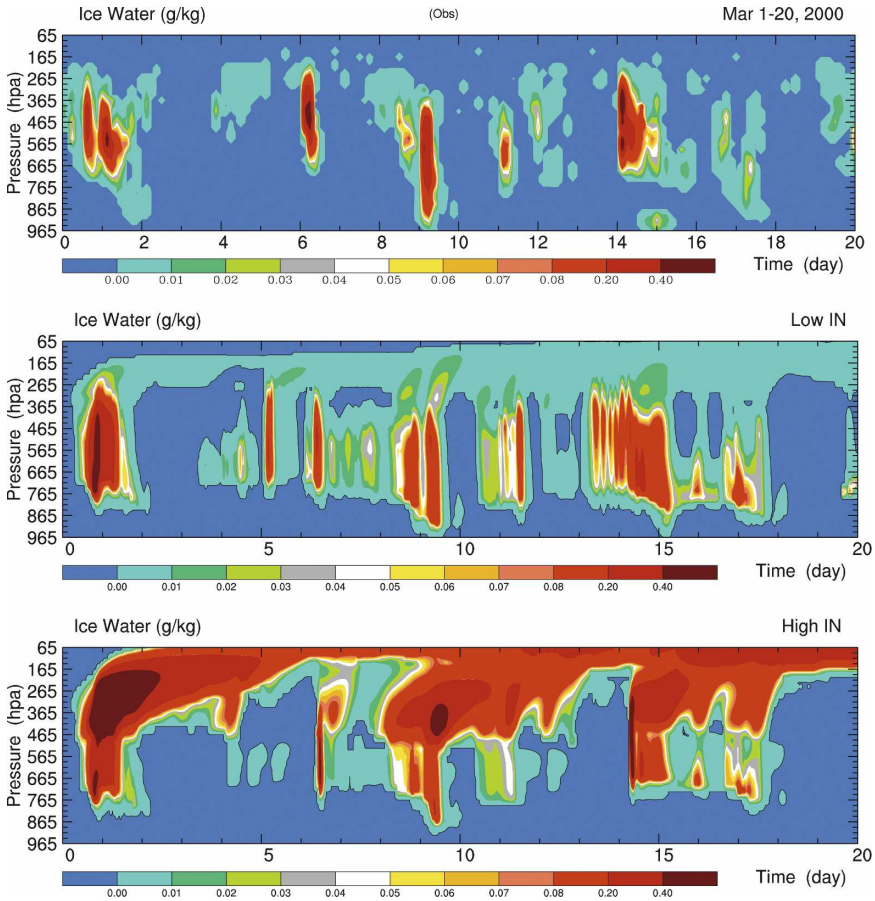

FIG. 15. Time–pressure cross sections of ice water content in the ARM-SGP-00 numerical experiments and field observations: results from (top) observation and (middle), (bottom) the experiments with low and high IN concentrations, respectively.

of the tropical ones. It shows that the effect of IN on the net radiative flux at the TOA in the middle latitudes differs significantly from that in the tropics. In midlatitudes, the flux increases with IN concentration first and then decreases, which is physically consistent.

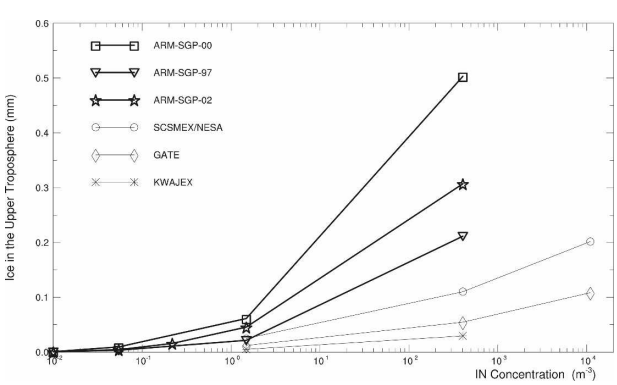

FIG. 16. Ice water content above 7.4 km vs the IN concentration at −10°C for all of the ARM-SGP numerical experiments (thick lines) and some of the tropical experiments (thin lines).

This differing sensitivity of the net radiative flux to IN concentration makes physical sense. Cirrus clouds decrease the upwelling infrared flux at the TOA and increase the reflected upward solar flux by a varying

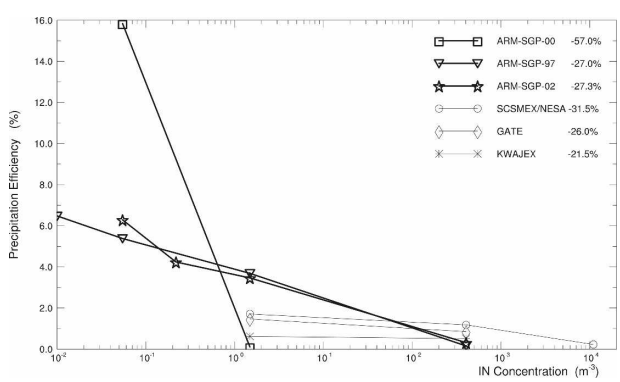

FIG. 17. Bulk precipitation efficiency of clouds vs the IN concentration at −10°C. Thick and thin lines represent the results for the midlatitudinal and tropical numerical experiments, respectively. The vertical axis represents the PE minus the value shown in the upper right corner.

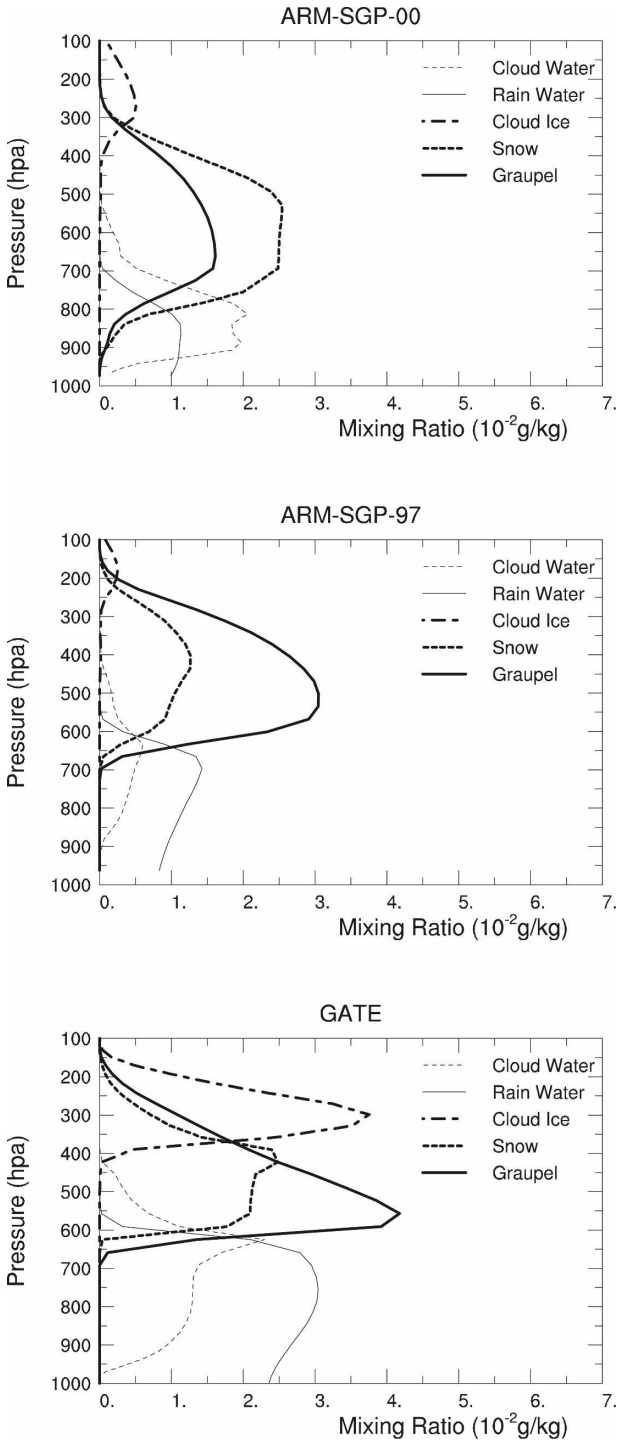

FIG. 18. Mean vertical profiles of ice species in the (top) ARM-SGP-00 and (middle) -97 experiments with low IN concentration and (bottom) the GATE experiment with high IN concentration.

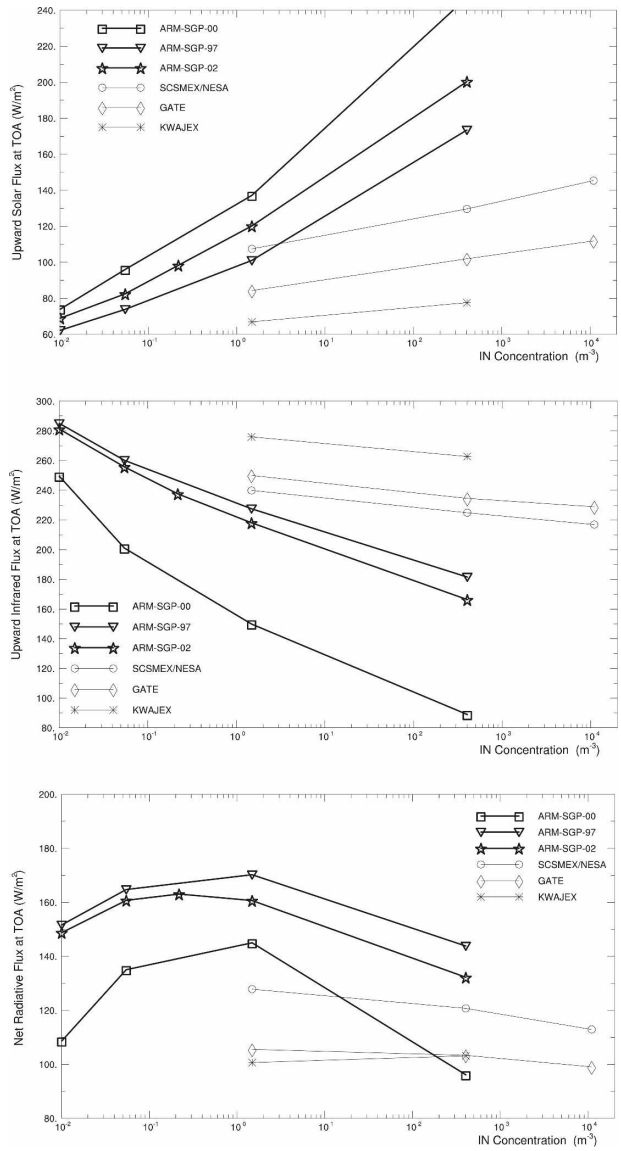

FIG. 19. (top) Upward solar flux, (middle) infrared, and (bottom) net radiative flux at the TOA vs the IN concentration at a temperature of −10°C (thick lines) for all of the ARM-SGP experiments and some of the tropical experiments (thin lines). The line for ARM-SGP-00 in the lower panel represents the result of the ARM-SGP-00 experiment plus 100 W m^{-2}.

magnitude that depends on the underlying cloud conditions and optical depth of the cirrus. When the UT ice content is very small, the upward infrared radiation at the TOA decreases significantly with increasing UT ice content, while at the same time the solar reflection increases, but to a lesser degree. As a result, the net downward radiative flux increases with increasing UT ice content.

In contrast, when the UT ice content is large, the net radiative flux decreases (or changes little) with increasing IN concentration. Solar reflection by cloud increases significantly with increasing cloud ice whereas the upward infrared flux emitted by cloud decreases to a lesser degree. As a result, the net downward flux

decreases with increasing IN concentration when the UT ice content is large.

6. Conclusions

Only one microphysics scheme is used to model cloud ensembles and their resulting radiation in both the midlatitudes and tropics. Nine field campaigns scattered over a broad area of the earth's surface are chosen to provide large-scale forcing data for CRM simulations. Classifying the CRM simulations into tropical and midlatitudinal and then comparing the types leads to the following conclusions:

1) The bulk PE of clouds decreases with increasing IN concentration in both the middle latitudes and tropics. This effect of IN on PE is physically clear. With increasing IN concentration, the conversion rate of cloud ice to snow decreases in the Bergeron process. As a result, the graupel embryos (or snow crystals) decrease in population and consequently so too does graupel riming. Hence, increasing IN in the middle troposphere brings about a decrease in PE and therefore an increase in UT cloud ice via updraft.
2) Because IN impact UT cloud ice, which in turn modulates solar and infrared radiation, IN indirectly affect the solar and infrared fluxes at the TOA and BOA. In all the numerical experiments carried out, the upward solar and infrared fluxes at the TOA increase and decrease with increasing IN concentration, respectively. In contrast, the solar and infrared fluxes at the BOA decrease and increase, respectively. Because the solar and infrared fluxes respond to IN concentration oppositely, the sensitivity of the net radiative fluxes to IN concentration at the TOA varies from one case to another.
3) The effect of IN on the radiative fluxes at the TOA and the UT cloud ice content is stronger in midlatitudes than in the tropics. This differing effect at different latitudes is physically consistent because graupel riming is relatively more important in tropical precipitation whereas the Bergeron process is more important in midlatitudinal precipitation.
4) This proposed indirect effect of IN on radiation, which corresponds to colloidal instability in the mixed-phase region, is the most prominent of all the effects investigated. Because IN concentration varies by several orders of magnitude (Fletcher 1962; Pruppacher and Klett 1997; DeMott et al. 2003), the comparison between model results and observations is used to diagnose ice particle concentration (or the active IN concentration times the ice crystal enhancement factor), and it reveals that the ice particle concentration in tropical clouds is much larger than in midlatitudinal ones. Hence, sufficient IN observations are necessary for future evaluation of CRM simulations.

Acknowledgments. This research was supported by the NASA Headquarters Atmospheric Dynamics and Thermodynamics Program and the NASA Tropical Rainfall Measuring Mission (TRMM). The research was also supported by the Office of Science (BER), U.S. Department of Energy/Atmospheric Radiation Measurement (DOE/ARM) Interagency Agreement DE-AI02–04ER63755. The authors are grateful to Dr. R. Kakar at NASA headquarters and Dr. Kiran Alapaty at DOE/ARM for their support of this research. The research was also supported by NASA and the DOE Atmospheric Radiation Measurement Program (ARM) to the Stony Brook University. Dr. Xie, working at LLNL, was supported under the auspices of the U.S. Department of Energy (DOE) Office of Science, Biological and Environmental Research by the University of California Lawrence Livermore National Laboratory under Contract W-7405-Eng-48.

The authors acknowledge the NASA Ames Research Center and the NASA Goddard Space Flight Center for enormous computer time used in this research. They also thank Dr. Gang Hong and two anonymous reviewers for their critical yet constructive comments.

REFERENCES

Ackerman, T. P., and G. M. Stokes, 2003: The Atmospheric Radiation Measurement Program. *Phys. Today,* **56,** 38–44.

Baker, M. B., 1997: Cloud microphysics and climate. *Science,* **276,** 1072–1078.

Bergeron, T., 1935: On the physics of clouds and precipitation. *Proc. 5th Assembly U.G.G.I.,* Lisbon, Portugal, International Union of Geodesy and Geophysics, 156–180.

Blossey, P. N., C. S. Bretherton, J. Cetrone, and M. Kharoutdino, 2007: Cloud-resolving model simulations of KWAJEX: Model sensitivities and comparisons with satellite and radar observations. *J. Atmos. Sci.,* **64,** 1488–1508.

Braham, R. R., 1952: The water and energy budgets of the thunderstorm and their relation to thunderstorm development. *J. Meteor.,* **9,** 227–242.

Bretherton, C. S., and A. H. Sobel, 2003: The Gill model and the weak temperature gradient approximation. *J. Atmos. Sci.,* **60,** 451–460.

——, P. N. Blossey, and M. Khairoutdinov, 2005: An energy-balance analysis of deep convective self-aggregation above uniform SST. *J. Atmos. Sci.,* **62,** 4273–4292.

Byers, H. R., and R. R. Braham Jr., 1948: Thunderstorm structure and circulation. *J. Meteor.,* **5,** 71–86.

Charney, J. G., 1979: *Carbon Dioxide and Climate: A Scientific Assessment.* National Academy of Sciences, 22 pp.

Ciesielski, P. E., R. H. Johnson, P. T. Haertel, and J. Wang, 2003: Corrected TOGA COARE sounding humidity data: Impact

on diagnosed properties of convection and climate over the warm pool. *J. Climate,* **16,** 2370–2384.

Cohen, B. G., and G. C. Craig, 2006: Fluctuations in an equilibrium convective ensemble. Part II: Numerical experiments. *J. Atmos. Sci.,* **63,** 2005–2015.

DeMott, P. J., D. J. Cziczo, A. J. Prenni, D. M. Murphy, S. M. Kreidenweis, D. S. Thomson, R. Borys, and D. C. Rogers, 2003: Measurements of the concentration and composition of nuclei for cirrus formation. *Proc. Natl. Acad. Sci. USA,* **100,** 14 655–14 660.

Ekman, A. M. L., A. Engström, and C. Wang, 2007: The effect of aerosol composition and concentration on the development and anvil properties of a continental deep convective cloud. *Quart. J. Roy. Meteor. Soc.,* **133,** 1439–1452.

Fletcher, N. H., 1962: *The Physics of Rain Clouds.* Cambridge University Press, 386 pp.

Grabowski, W. W., 2001: Coupling cloud processes with the large-scale dynamics using the cloud-resolving convection parameterization (CRCP). *J. Atmos. Sci.,* **58,** 978–997.

——, X. Wu, M. W. Moncrieff, and W. D. Hall, 1998: Cloud-resolving modeling of cloud systems during Phase III of GATE. Part II: Effects of resolution and the third spatial dimension. *J. Atmos. Sci.,* **55,** 3264–3282.

——, ——, and ——, 1999: Cloud-resolving modeling of tropical cloud systems during Phase III of GATE. Part III: Effects of cloud microphysics. *J. Atmos. Sci.,* **56,** 2384–2402.

Hallett, J., and S. C. Mossop, 1974: Production of secondary ice particles during the riming process. *Nature,* **249,** 26–28.

Hartmann, D. L., M. E. Ockert-Bell, and M. L. Michelsen, 1992: The effect of cloud type on the earth's energy balance: Global analysis. *J. Climate,* **5,** 1281–1304.

Heymsfield, A. J., and L. J. Donner, 1990: A scheme for parameterizing ice-cloud water content in general circulation models. *J. Atmos. Sci.,* **47,** 1865–1877.

——, and J. Iaquinta, 2000: Cirrus crystal terminal velocities. *J. Atmos. Sci.,* **57,** 916–938.

Hong, S.-Y., J. Dudhia, and S.-H. Chen, 2004: A revised approach to ice-microphysical processes for the bulk parameterization of cloud and precipitation. *Mon. Wea. Rev.,* **132,** 103–120.

Hsie, E. Y., R. D. Farley, and H. D. Orville, 1980: Numerical simulation of ice-phase convective cloud seeding. *J. Appl. Meteor.,* **19,** 950–977.

Johnson, D. E., W.-K. Tao, J. Simpson, and C.-H. Sui, 2002: A study of the response of deep tropical clouds to large-scale thermodynamic forcing. Part I: Modeling strategies and simulations of TOGA COARE convective systems. *J. Atmos. Sci.,* **59,** 3492–3518.

Johnson, R. H., and P. E. Ciesielski, 2002: Characteristics of the 1998 summer monsoon onset over the northern South China Sea. *J. Meteor. Soc. Japan,* **80,** 561–578.

Khairoutdinov, M. F., and D. A. Randall, 2001: A cloud-resolving model as a cloud parameterization in the NCAR Communicate Climate System Model: Preliminary results. *Geophys. Res. Lett.,* **28,** 3617–3620.

——, and ——, 2003: Cloud-resolving modeling of the ARM summer 1997 IOP: Model formulation, results, uncertainties, and sensitivities. *J. Atmos. Sci.,* **60,** 607–625.

——, ——, and C. DeMott, 2005: Simulations of the atmospheric general circulation using a cloud-resolving model as a superparameterization of physical processes. *J. Atmos. Sci.,* **62,** 2136–2154.

Klemp, J. B., and R. B. Wilhelmson, 1978: The simulation of three-dimensional convective storm dynamics. *J. Atmos. Sci.,* **35,** 1070–1096.

Koenig, L. R., 1971: Numerical modeling of ice deposition. *J. Atmos. Sci.,* **28,** 226–237.

Korolev, A. V., and I. P. Mazin, 2003: Supersaturation of water vapor in clouds. *J. Atmos. Sci.,* **60,** 2957–2974.

Lang, S., W.-K. Tao, R. Cifelli, W. Olson, J. Halverson, S. Rutledge, and J. Simpson, 2007: Improving simulations of convective systems from TRMM LBA: Easterly and westerly regimes. *J. Atmos. Sci.,* **64,** 1141–1164.

Lau, K.-M., C.-H. Sui, M.-D. Chou, and W.-K. Tao, 1994: An inquiry into the cirrus-cloud thermostat effect for tropical sea surface temperature. *Geophys. Res. Lett.,* **21,** 1157–1160.

——, and Coauthors, 2000: A report of the field operations and early results of the South China Sea Monsoon Experiment (SCSMEX). *Bull. Amer. Meteor. Soc.,* **81,** 1261–1270.

Lin, Y.-L., R. D. Farley, and H. D. Orville, 1983: Bulk parameterization of the snow field in a cloud model. *J. Climate Appl. Meteor.,* **22,** 1065–1092.

Liu, C., and M. W. Moncrieff, 2001: Cumulus ensemble in shear: Implications for parameterization. *J. Atmos. Sci.,* **58,** 2832–2842.

Lohmann, U., and J. Feichter, 2005: Global indirect aerosol effects: A review. *Atmos. Chem. Phys.,* **5,** 715–737.

Matsui, T., X. Zeng, W.-K. Tao, S. Lang, M. Zhang, and H. Masunaga, 2007: Evaluation of microphysics and precipitation-type frequencies in long-term cloud-resolving model simulations using the TRMM satellite. *Proc. 2007 Fall AGU Joint Assembly,* San Francisco, CA, Amer. Geophys. Union.

Meyers, M. P., P. J. Demott, and W. R. Cotton, 1992: New primary ice-nucleation parameterizations in an explicit cloud model. *J. Appl. Meteor.,* **31,** 708–721.

Miller, M. A., K. L. Johnson, D. T. Troyan, E. E. Clothiaux, E. J. Mlawer, and G. G. Mace, 2003: ARM value-added cloud products: Description and status. *Proc. 13th ARM Science Team Meeting,* Washington, DC, U.S. Dept of Energy. [Available online at http://www.arm.gov/publications/proceedings/conf13/extended_abs/miller-ma.pdf.]

National Research Council, 2005: *Radiative Forcing of Climate Change: Expanding the Concept and Addressing Uncertainties.* National Academy of Sciences, 224 pp.

Ooyama, K., 1987: Scale-controlled objective analysis. *Mon. Wea. Rev.,* **115,** 2476–2506.

Paluch, I. R., 1979: The entrainment mechanism in Colorado cumuli. *J. Atmos. Sci.,* **36,** 2467–2478.

Petch, J. C., and M. E. B. Gray, 2001: Sensitivity studies using a cloud-resolving model simulation of the tropical west Pacific. *Quart. J. Roy. Meteor. Soc.,* **127,** 2287–2306.

Phillips, V. T. J., and L. J. Donner, 2006: Cloud microphysics, radiation and vertical velocities in two- and three-dimensional simulations of deep convection. *Quart. J. Roy. Meteor. Soc.,* **132,** 3011–3033.

——, ——, and S. T. Garner, 2007: Nucleation processes in deep convective simulated by a cloud-system-resolving model with double-moment bulk microphysics. *J. Atmos. Sci.,* **64,** 738–761.

Pruppacher, H. R., and J. D. Klett, 1997: *Microphysics of Clouds and Precipitation.* 2nd ed. Kluwer Academic, 954 pp.

Randall, D., M. Khairoutdinov, A. Arakawa, and W. Grabowski, 2003: Breaking the cloud parameterization deadlock. *Bull. Amer. Meteor. Soc.,* **84,** 1547–1564.

Raymond, D. J., and X. Zeng, 2005: Modelling tropical atmo-

spheric convection in the context of the weak temperature gradient approximation. *Quart. J. Roy. Meteor. Soc.,* **131,** 1301–1320.

Riehl, H., and J. S. Malkus, 1958: On the heat balance in the equatorial trough zone. *Geophysica,* **6,** 503–538.

Robe, F. R., and K. A. Emanuel, 1996: Moist convective scaling: Some inferences from three-dimensional cloud ensemble simulations. *J. Atmos. Sci.,* **53,** 3265–3275.

——, and ——, 2001: The effect of vertical wind shear on radiative–convective equilibrium states. *J. Atmos. Sci.,* **58,** 1427–1445.

Rogers, R. R., and M. K. Yau, 1989: *A Short Course in Cloud Physics.* 3rd ed. Butterworth-Heinemann, 290 pp.

Rutledge, S. A., and P. V. Hobbs, 1984: The mesoscale and microscale structure and organization of clouds and precipitation in midlatitude cyclones. XII: A diagnostic modeling study of precipitation development in narrow cold-frontal rainbands. *J. Atmos. Sci.,* **41,** 2949–2972.

Simpson, J., and W.-K. Tao, 1993: The Goddard Cumulus Ensemble model. Part II: Applications for studying cloud precipitating processes and for NASA TRMM. *Terr. Atmos. Oceanic Sci.,* **4,** 73–116.

——, R. F. Adler, and G. R. North, 1988: A proposed Tropical Rainfall Measuring Mission (TRMM) satellite. *Bull. Amer. Meteor. Soc.,* **69,** 278–295.

Smolarkiewicz, P. K., and W. W. Grabowski, 1990: The multidimensional positive advection transport algorithm: Nonoscillatory option. *J. Comput. Phys.,* **86,** 355–375.

Sobel, A. H., and C. S. Bretherton, 2000: Modeling tropical precipitation in a single column. *J. Climate,* **13,** 4378–4392.

Soong, S.-T., and Y. Ogura, 1980: Response of trade wind cumuli to large-scale processes. *J. Atmos. Sci.,* **37,** 2035–2050.

Starr, D. O'C., and S. K. Cox, 1985: Cirrus clouds. Part I: A cirrus cloud model. *J. Atmos. Sci.,* **42,** 2663–2681.

Sui, C.-H., K.-M. Lau, W.-K. Tao, and J. Simpson, 1994: The tropical water and energy cycles in a cumulus ensemble model. Part I: Equilibrium climate. *J. Atmos. Sci.,* **51,** 711–728.

Tao, W.-K., 2003: Goddard cumulus ensemble (GCE) model: Application for understanding precipitating processes. *Cloud Systems, Hurricanes, and the Tropical Rainfall Measuring Mission (TRMM), Meteor. Monogr.,* No. 51, 107–138.

——, and J. Simpson, 1993: The Goddard Cumulus Ensemble model. Part I: Model description. *Terr. Atmos. Oceanic Sci.,* **4,** 35–72.

——, S. Lang, J. Simpson, C.-H. Sui, B. Ferrier, and M.-D. Chou, 1996: Mechanisms of cloud–radiation interaction in the tropics and midlatitudes. *J. Atmos. Sci.,* **53,** 2624–2651.

——, J. Simpson, C.-H. Sui, C.-L. Shie, B. Zhou, K. M. Lau, and M. Moncrieff, 1999: Equilibrium states simulated by cloud-resolving models. *J. Atmos. Sci.,* **56,** 3128–3139.

——, and Coauthors, 2003a: Microphysics, radiation and surface processes in the Goddard Cumulus Ensemble (GCE) model. *Meteor. Atmos. Phys.,* **82,** 97–137.

——, C.-L. Shie, J. Simpson, S. Braun, R. H. Johnson, and P. E. Ciesielski, 2003b: Convective systems over the South China Sea: Cloud-resolving model simulations. *J. Atmos. Sci.,* **60,** 2929–2956.

——, D. Johnson, C.-L. Shie, and J. Simpson, 2004: Atmospheric energy budget and large-scale precipitation efficiency of convective systems during TOGA COARE, GATE, SCSMEX, and ARM: Cloud-resolving model simulations. *J. Atmos. Sci.,* **61,** 2405–2423.

——, and Coauthors, 2009: A multiscale modeling system: Developments, applications, and critical issues. *Bull. Amer. Meteor. Soc.,* in press.

Tompkins, A. M., and G. C. Craig, 1998: Radiative–convective equilibrium in a three-dimensional cloud ensemble model. *Quart. J. Roy. Meteor. Soc.,* **124,** 2073–2098.

Webster, P. J., and R. Lukas, 1992: TOGA COARE: The Coupled Ocean–Atmosphere Response Experiment. *Bull. Amer. Meteor. Soc.,* **73,** 1377–1416.

Wu, X., and M. W. Moncrieff, 2001: Long-term behavior of cloud systems in TOGA COARE and their interactions with radiative and surface processes. Part III: Effects on the energy budget and SST. *J. Atmos. Sci.,* **58,** 1155–1168.

——, W. W. Grabowski, and M. W. Moncrieff, 1998: Long-term behavior of cloud systems in TOGA COARE and their interactions with radiative and surface processes. Part I: Two-dimensional modeling study. *J. Atmos. Sci.,* **55,** 2693–2714.

——, W. D. Hall, W. W. Grabowski, M. W. Moncrieff, W. D. Collins, and J. T. Kiehl, 1999: Long-term behavior of cloud systems in TOGA COARE and their interactions with radiative and surface processes. Part II: Effects of ice microphysics on cloud–radiation interaction. *J. Atmos. Sci.,* **56,** 3177–3195.

——, S. Park, and Q. Min, 2008: Seasonal variation of cloud systems over ARM SGP. *J. Atmos. Sci.,* **65,** 2107–2129.

Xie, S., and Coauthors, 2002: Intercomparison and evaluation of cumulus parametrizations under summertime midlatitude continental conditions. *Quart. J. Roy. Soc.,* **128,** 1095–1135.

——, and Coauthors, 2005: Simulations of midlatitude frontal clouds by single-column and cloud-resolving models during the Atmospheric Radiation Measurement March 2000 cloud intensive operational period. *J. Geophys. Res.,* **110,** D15S03, doi:10.1029/2004JD005119.

Xu, K.-M., and D. A. Randall, 1996: Explicit simulation of cumulus ensembles with the GATE phase III data: Comparison with observations. *J. Atmos. Sci.,* **53,** 3710–3736.

——, and Coauthors, 2002: An intercomparison of cloud-resolving models with the Atmospheric Radiation Measurement summer 1997 intensive observation period data. *Quart. J. Roy. Meteor. Soc.,* **128,** 593–624.

——, and Coauthors, 2005: Modeling springtime shallow frontal clouds with cloud-resolving and single-column models. *J. Geophys. Res.,* **110,** D15S04, doi:10.1029/2004JD005153.

Zeng, X., and D. J. Raymond, 1999: Numerical simulation of radiative–convective equilibrium in the tropical atmosphere. Preprints, *23rd Conf. on Hurricane and Tropical Meteorology,* Dallas, TX, Amer. Meteor. Soc., 776–778.

——, and Coauthors, 2007a: Evaluating clouds in long-term cloud-resolving model simulations with observational data. *J. Atmos. Sci.,* **64,** 4153–4177.

——, W.-K. Tao, M. Zhang, S. Xie, and J. Simpson, 2007b: Modeling the effect of ice nuclei on ARM clouds. *Proc. 2007 ARM Cloud Properties and Cloud Modeling Joint WG Meeting,* Annapolis, MD, Amer. Geophys. Union.

——, ——, S. Lang, A. Y. Hou, M. Zhang, and J. Simpson, 2008: On the sensitivity of atmospheric ensembles to cloud microphysics in long-term cloud-resolving model simulations. *J. Meteor. Soc. Japan,* in press.

Zhang, M. H., and J. L. Lin, 1997: Constrained variational analysis of sounding data bases on column-integrated budgets of mass, heat, moisture, and momentum: Approach and application to ARM measurements. *J. Atmos. Sci.,* **54,** 1503–1524.

——, ——, R. T. Cederwall, J. J. Yio, and S. C. Xie, 2001: Objective analysis of ARM IOP data: Method and sensitivity. *Mon. Wea. Rev.,* **129,** 295–311.

Zhang, R., G. Li, J. Fan, D. L. Wu, and M. J. Molina, 2007: Intensification of Pacific storm track linked to Asian pollution. *Proc. Natl. Acad. Sci. USA,* **104,** 5295–5299.

Zhou, Y., and Coauthors, 2007: Use of high-resolution satellite observations to evaluate cloud and precipitation statistics from cloud-resolving model simulations. Part I: South China Sea Monsoon Experiment. *J. Atmos. Sci.,* **64,** 4309–4329.